



Original Research Article



Tongue squamous cell carcinoma-derived exosomes miR-21-5p affect tumor progression via promoting M2 macrophage polarization

Zixian Xu^{a,b,1} , Xin Fang^{b,d,1}, Shan Wang^a, Jiabei Mu^a, Qixian Gai^{a,b},
Yantong Chen^{a,b}, Zheyi Sun^{b,c,*}, Jiemei Zhai^{a,d,**} 

^a Department of Basic Science of Stomatology, Kunming Medical University School and Hospital of Stomatology, 1168 Chunrong West Road, Chenggong Zone, Kunming, 650500, China

^b Yunnan Key Laboratory of Stomatology, 1168 Chunrong West Road, Chenggong Zone, Kunming, 650500, China

^c Department of Endodontics, Kunming Medical University School and Hospital of Stomatology, 1088 Middle Haiyuan Road, High-Tech Zone, Kunming, 650106, China

^d Oral Medicine, Kunming Medical University School and Hospital of Stomatology, 1088 Middle Haiyuan Road, High-Tech Zone, Kunming, 650106, China

ARTICLE INFO

Keywords:

Tongue squamous cell carcinoma
Exosome
miR-21-5p
M2-type macrophage

ABSTRACT

Exosome-mediated intercellular communication plays a key role in shaping the tumor microenvironment and promoting tumor progression. Recent studies have demonstrated that tumor exosomal miRNAs significantly contribute to the polarization of tumor-associated macrophages (TAMs). However, the molecular mechanisms underlying miRNA-mediated regulation of macrophage polarization by exosomes derived from tongue squamous cell carcinoma (TSCC) remain incompletely elucidated. In this study, small RNA sequencing analysis of exosomal miRNAs revealed miR-21-5p was highly expressed in TSCC-derived exosomes. Further investigation demonstrated a significant association between exosomal miR-21-5p and M2 polarization of tumor-associated macrophages (TAMs). Functionally, TSCC-derived exosomes promoted the polarization of M0 macrophages towards the M2 phenotype. Mechanistically, exosomal miR-21-5p enhanced M2 polarization of TAMs by inhibiting phosphorylation of ERK1/2. Additionally, we performed single-sample gene set enrichment analysis (ssGSEA), constructed a multivariate Cox regression model, and performed survival analysis using paired RNA transcriptome and clinical data from TSCC patients. Our results revealed a significant enrichment of M2 macrophages in the tumor microenvironment (TME) of TSCC compared to adjacent normal tissue. Furthermore, we confirmed that M2 macrophages infiltration is associated with poor prognosis in TSCC patients. In summary, our study demonstrates that TSCC-derived exosomal miR-21-5p plays a critical role in M2 macrophage polarization, and M2 macrophages infiltration contributes to the progression of TSCC. Therefore, these findings suggest that therapeutic targeting of miR-21-5p may represent a novel strategy for TSCC treatment by selectively modulating the M2 polarization of TAMs.

1. Introduction

Tongue squamous cell carcinoma (TSCC), the most common oral cancer, exhibits a higher biological aggressiveness and worse clinical outcomes compared to other parts of the oral cavity due to the frequent mechanical movement of the tongue and the rich blood and lymphatic circulation [1–4]. Thus, exploring the molecular mechanisms of TSCC, developing effective therapeutic strategies, preventing the metastatic

progression, and improving survival outcomes and quality of life for patients are urgent problems that need to be addressed.

Tumor-associated macrophages (TAMs), as a major component of the immunosuppressive tumor microenvironment, have garnered increasing attention in recent years. TAMs are categorized into classically activated M1 and alternatively activated M2 phenotypes based on their morphological, phenotypic and functional heterogeneity [5,6]. During tumor progression, monocytes are recruited into the tumor microenvironment

Peer review under the responsibility of Editorial Board of Non-coding RNA Research.

* Corresponding author. Yunnan Key Laboratory of Stomatology, 1168 Chunrong West Road, Chenggong Zone, Kunming, 650500, China.

** Corresponding author. Department of Basic Science of Stomatology, Kunming Medical University School and Hospital of Stomatology, 1168 Chunrong West Road, Chenggong Zone, Kunming, 650500, China.

E-mail addresses: sunzheyi@kmmu.edu.cn (Z. Sun), zhaijiemei@kmmu.edu.cn (J. Zhai).

¹ Zixian Xu and Xin Fang contribute equally as first authors.

<https://doi.org/10.1016/j.ncrna.2025.05.006>

Received 25 February 2025; Received in revised form 25 April 2025; Accepted 15 May 2025

Available online 15 May 2025

2468-0540/© 2025 The Authors. Publishing services by Elsevier B.V. on behalf of KeAi Communications Co. Ltd. This is an open access article under the CC BY-NC-ND license (<http://creativecommons.org/licenses/by-nc-nd/4.0/>).

by cytokines or chemokines, where they primarily differentiate into the M2-polarized subtype [7]. TAMs promote tumor progression through multiple mechanisms, including enhancing cancer cell proliferation and migration, facilitating immune evasion, and suppressing apoptosis [8]. Therefore, investigating the mechanisms underlying M2 polarization in the tumor microenvironment and targeting M2-polarized macrophages represents a promising therapeutic strategies.

Exosomes are membrane-bound extracellular vesicles (30–150 nm in diameter) characterized by a phospholipid bilayer structure and function as key mediators of intercellular communication. Research on exosomes has undergone substantial expansion, with particular emphasis on their roles in the areas of non-coding RNAs, immunity, stem cells, and targeted cancer therapy [9–11]. The exosomal cargo is composed of diverse biomolecular constituents including proteins, lipids, DNA, mRNAs, and various non-coding RNAs [12]. Notably, microRNAs (miRNAs) constitute essential exosomal components that regulate the expression of protein-coding genes by binding directly to their targets in a sequence-specific manner [13]. Accumulating evidence indicates that exosomal miRNAs can induce M2 polarization of macrophages [14–16]. Furthermore, accumulating evidence indicates that tumor-derived exosomal miRNAs critically promote polarization of M2 macrophages and accelerate tumor progression across multiple malignancies, including lung adenocarcinoma, gastric cancer, liver cancer, etc [17–20]. However, the precise mechanisms by which TSCC-derived exosomal miRNAs affect macrophage polarization remain incompletely characterized, warranting further exploration.

In this study, we identified that tumor-derived exosomes from TSCC cells induced M0-to-M2 macrophage polarization. Through systematic bioinformatics analysis, we constructed a prognostic Cox regression model incorporating M2 macrophage-associated markers, which showed strong predictive performance for clinical outcomes in TSCC patients. Mechanistic investigations revealed that exosomal miR-21-5p mediated macrophage M2 polarization process through modulation of the ERK1/2 signaling pathway. These results highlight that targeted inhibition of miR-21-5p may represent a promising therapeutic approach to impair M2 polarization in TSCC.

2. Materials and methods

2.1. Cell culture

The CAL27 cell line (RRID:CVCL_1107) was provided by the Yunnan Institute of Stomatology; The SCC9 (RRID:CVCL_1685), a human tongue squamous cell carcinoma cell line, was obtained from Wuhan Ponosi Biotechnology Co., Ltd.; The THP-1 (RRID:CVCL_0006) human monocyte macrophage leukemia cell line was acquired from Beina Biotechnology Co., Ltd. All cell lines were authenticated through the NCBI database to confirm their identity and exclude potential misidentification.

Declaration: All experimental protocols and procedures were reviewed and approved by the Medical Ethics Committee of the Affiliated Stomatological Hospital of Kunming Medical University (KYKQ2022MEC0098).

The CAL27 cells were cultured in Dulbecco's Modified Eagle Medium (DMEM, high glucose) supplemented with 10 % fetal bovine serum (Evacell, Hong Kong, China) and 1 % penicillin-streptomycin (Beyotime, China). The THP-1 cells were cultured in RPMI 1640 medium (Gibco, USA) containing 10 % fetal bovine serum (Gibco, USA), 1 % penicillin-streptomycin, and 0.1 % β -mercaptoethanol (Procell, China). The SCC9 cells were cultured in a cell-specific medium (Procell, China).

For exosome extraction experiments, TSCC cells were cultured in complete medium (DMEM/F12 for SCC9) supplemented with exosome-depleted FBS (Evacell, Hong Kong, China) until reaching approximately 50 % confluence. The supernatant was collected when cells reached 90–95 % confluence, centrifuged at 1200 rpm for 5 min, and filtered through a 0.22 μ m filter (Biosharp, China). The filtrate was then

concentrated using ultrafiltration tubes (Millipore, USA), followed by exosome isolation using the Exo-easy Exosome Extraction Kit (Qiagen, Germany).

In the macrophage polarization assay, THP-1 cells were initially differentiated into M0-type macrophages by treatment with 100 ng/mL phorbol 12-myristate 13-acetate (PMA) for 48 h, followed by M2 polarization stimulation with 0, 25, 50, or 100 μ g/mL TSCC-derived exosomes for another 48 h. Positive controls consisted of IL-4 (20 ng/mL) and IL-13 (20 ng/mL), while THP-1 cells cultured in complete medium served as the negative control.

To prepare M2 macrophage-conditioned medium, M2-polarized macrophages were cultured in serum-free RPMI 1640 medium for 24 h to collect cells supernatant. The collected supernatant was subjected to 1200 rpm for 5 min and subsequently filtered through a 0.22 μ m filter. The resulting conditioned medium was diluted in a 1:2 ratio with fresh serum-free medium.

To assess cisplatin-induced apoptosis in TSCC cells, the cells were exposed to graded concentrations of cisplatin (1, 2, 4, and 8 μ M) for 24, 48 and 72 h, cell viability was measured, and the half-maximal inhibitory concentration (IC50) was determined using nonlinear regression analysis.

To activate ERK1/2 signaling, cells were stimulated with the specific ERK1/2 agonist HY-W010907 (Medchemexpress, USA) at 65 nM for 24h to induce upregulation of phosphorylated ERK1/2 (p-ERK1/2) levels.

2.2. Western blot

Total protein lysates (10 μ g per lane) were resolved by 10 % SDS-polyacrylamide gel electrophoresis (SDS-PAGE) and transferred onto a polyvinylidene fluoride (PVDF) membranes. Exosome markers: CD9 (Huaxingbio, China), CD81 (Huaxingbio, China), HSP90 (Huaxingbio, China), Calnexin (Huaxingbio, China). MAPK pathway proteins: ERK1/2 (Nature Biosciences, China), p-ERK1/2 (Nature Biosciences, China), JNK1/2/3 (Huaxingbio, China), p-JNK1/2/3 (Huaxingbio, China), P38 MAPK (Wanleibio, China), p-P38 MAPK (Wanleibio, China), GAPDH (Proteintech, China). After incubation with goat anti-rabbit or anti-mouse secondary antibodies (Huaxingbio, China), protein bands were visualized using the Omni-ECL™ Ultrasensitive Chemiluminescence Detection Kit (Epizyme, China). All primary antibodies were diluted 1:1000.

2.3. Flow cytometry

For immunophenotyping, M0-type macrophages were stained with PE-CD14 and FITC-CD11b (BioLegend) antibodies. For apoptosis analysis, TSCC cells treated with cisplatin were dual-stained with Annexin V-FITC and propidium iodide. All samples were acquired on a NovoCyte D2040R flow cytometer (Agilent, USA), and data were analyzed using FlowJo software (v10.8.1, BD Biosciences).

2.4. Immunofluorescence

For membrane labeling, Exosomes or M0-type macrophage cell membranes were incubated with PKH26 (Solarbio, China) staining solution. For intracellular tracking experiments, GFP-tagged miR-21-5p mimics were transfected into target cells, followed by nuclear counterstaining with DAPI. Confocal imaging was performed using a laser confocal microscope (Nikon, Japan) and fluorescence signals were quantified with NIS-Elements Viewer 5.

2.5. Total RNA extraction and qPCR

Total RNA was isolated using the SteadyPure Rapid RNA Extraction Kit (Agbio, China). Reverse transcription and real-time PCR was conducted using the Evo M-MLV Reverse Transcription Premixed Kit (Agbio, China) and the SYBR® Green Pro Taq HS Premixed qPCR Kit

(with Rox) (Agbio, China), respectively.

Sequences for primer design and synthesis can be found in Table 1.

2.6. EdU proliferation

CAL27/SCC9 cells were seeded in confocal dishes (Nest, China) at a density of 5×10^5 cells per dish, and subsequently treated with prepared M2 conditioned medium for 24 h. Fluorescence imaging was performed using a laser confocal microscope (Nikon, Japan).

2.7. Transwell invasion experiments

Gold Medal Matrix Gel ABW (Corning, USA) was prepared by combining the base medium at a ratio of 1:8 to prepare the matrix gel mixture. 60 μ L of the matrix solution uniformly coated onto the upper chamber of a transwell chamber (8 μ m pore size, 24-well plate, Corning) and polymerized for 3 h at 37 °C in an incubator. The gel-coated membranes were then equilibrated with 100 μ L of serum-free medium. CAL27/SCC9 cell suspensions (1.5×10^4 cells per chamber in 200 μ L conditioned medium) were seeded into the upper chambers, while the lower chambers contained 700 μ L complete medium supplemented with 20 % FBS. Following 48 h incubation (24 h for SCC9), non-invading cells were removed from the upper membrane surface. Migrated cells were fixed with absolute methanol and stained with 1 % crystal violet solution (Beyotime Biotechnology, Inc. C0121). Cell quantification analysis was performed in 5 random fields.

2.8. Scratch test

CAL27/SCC9 cells were seeded in 6-well plates (Nest, China) at a density of 1×10^6 cells per well. When the cell confluence reached 90 %–95 %, a standardized wound was drawn with a 10 μ L pipette tip perpendicular to the plate surface. After removing culture medium, gently rinse the wound area with sterile phosphate-buffered saline (PBS) to remove detached cellular debris. Cells were then treated with M2 macrophage-conditioned medium (prepared at a 1:2 ratio of M2 macrophage culture supernatant to complete growth medium). Subsequently, the cells were observed and photographed at 0, 24, and 48 h, respectively (0, 6, and 12 h for SCC9, initial observations at 24 h revealed complete closure of the scratch wound in SCC9 cells. Based on preliminary experimental optimization, subsequent time points were adjusted to 0, 6, and 12 h to better capture the dynamic migration process).

2.9. Bioinformatics analysis

The transcriptome sequencing data of tumor tissues and paired clinical data from patients with tongue squamous cell carcinoma (TSCC) were downloaded from The Cancer Genome Atlas (TCGA) database, including 148 TSCC cases and 15 matched adjacent normal tissues. Data processing was performed using RStudio, with count and TPM formats extracted for subsequent differential expression analysis and immune infiltration analysis, correspondingly. The Single-sample Gene Set Enrichment Analysis (ssGSEA) method was implemented to quantify the enrichment scores of 29 immune cell types in TSCC. These scores were

then visualized using box plots, generated with the R package "ggplot2", to compare immune infiltration levels between TSCC and paired adjacent normal tissues.

A table of immune cell markers was obtained from the Cellmarker 2.0 database (<http://117.50.127.228/CellMarker/>). Focusing on M2-type macrophage-associated markers ($n = 76$), we performed Least Absolute Shrinkage and Selection Operator (LASSO) regression with the penalty parameter (λ) set to lambda-min to identify core prognostic markers. These markers were then incorporated into a multivariate Cox regression model to establish an M2 macrophage-related gene signature for predicting patient survival outcomes. Using this model, the "Survival" package was applied to compute the hazard ratios (HR) of different samples, and classifying them into two groups of M2 "high risk" and M2 "low risk" samples based on the median HR value. Subsequent differential gene expression analysis between the two subgroups was performed using the DESeq2 package, followed by functional enrichment analyses including Gene Ontology (GO), Kyoto Encyclopedia of Genes and Genomes (KEGG) pathway analysis, and Gene Set Enrichment Analysis (GSEA) implemented through the ClusterProfiler package. These comprehensive bioinformatics approaches collectively enabled the elucidation of potential molecular mechanisms underlying the influence of M2-type macrophages on patient prognosis.

2.10. MicroRNA sequencing of exosomes

The exosomal miRNA sequencing was performed by Beijing Novozymes Biotechnology Co., Ltd. (Project No:X101SC21112373-Z01-J003, detailed sequencing methodology can be found in the supplementary data). Bioinformatics analysis identified miR-21-5p as the key candidate miRNA, with its potential targets were predicted using the "multiMir" R package. Subsequently, the targets were further analyzed through KEGG signaling pathway enrichment.

2.11. Cell transfection

CAL27, SCC9, or M0 cells (5×10^5 cells/dish) were seeded onto 15 mm confocal dishes and transfected with GFP fluorescent miR-21-5p mimics purchased from Beijing Dona Pharmaceutical Technology Co. The mimics were delivered into cells using CALNPTM RNAi in vitro transfection reagent (D-nano, China) following the manufacturer's instructions. Images were captured with a fluorescence microscope 24 h after transfection.

2.12. Statistical analysis

Data were processed using GraphPad Prism 9 software (GraphPad Software, San Diego, CA). Results are presented as mean \pm SEM. Statistical significance was determined using a two-tailed Student's *t*-test or two-way ANOVA.

Table 1
Sequences.

Gene	Forward	Reverse
IL1 β	TGGCTTATTACAGTGGCAATGAGG	AGTGGTGGTCGGAGATTCGTAG
TNF α	CCGCATCGCGTCTCCTAC	CGCTGAGTCGGTCACCCCTTC
INOS	ATCCAGCCGTGCCACCATC	CCATCCACCCTCGCTCCAG
ARG1	AAGGTGGCAGAAGTCAAGAAGAAC	TTGTGGTTGTCAGTGGAGTGTG
TGF β	GCAACAATTCTGGCGATACCTC	CCTCCACGGCTCAACCACTG
IL10	CTGTCTGGAGGACTTTAAGGGTTAC	CTGTATGCTGGGTTCTGGTTCTC
CD206	CGGTCCGGATGGATGGCTCTG	GCGGATTTGGAGTTTATCTGGTAG

3. Results

3.1. Exosomes from TSCC cells promote M2-type polarization of tumor-associated macrophages

In this part, we isolated the exosomes of the human TSCC cell lines CAL27 and SCC9. Transmission electron microscope revealed that the exosomes from CAL27 and SCC9 cells exhibited a "cup-shaped" double membrane structure (Fig. 1A). Nanoparticle tracking analysis (NTA) of the exosomes showed that the majority of particles were in the range of 30–150 nm in diameter, consistent with the size of exosomes (Fig. 1B). Western blot results confirmed the presence of established exosomal markers (CD9, CD81, and HSP90), with negligible expression of Calnexin, confirming the typical exosomal markers (Fig. 1C).

Next, We induced THP-1 monocyte differentiation into M0 macrophages using phorbol 12-myristate 13-acetate (PMA). Flow cytometry analysis showed that as the induction time prolongs, CD14 expression first slightly decreased and then increased. However, only 41.0% of cells significantly expressed CD11b at 24 h, while the expression of CD11b exceeded 70% at both 48h and 72h, indicating that THP-1 cells had successfully differentiated into M0 macrophages (Fig. 1D and E). Based on these findings, we selected 48h as the subsequent experimental condition for induction of M0-type macrophages.

To explore whether exosomes could be taken up by M0-type macrophages, we performed uptake assays and observed that CAL27-derived exosomes reached peak uptake after 12 h, while those from SCC9 reached peak uptake after 6 h (Fig. 1F and G).

To evaluate the role of exosomes in macrophage polarization, we quantified the mRNA expression of M2 and M1 markers in M0-type macrophages following 48h exosome co-culture. M0-type macrophages co-cultured with exosomes suppressed the expression of M1 markers including IL-1 β , TNF- α , or INOS, and increased the expression of M2 markers including Arg1, TGF- β , IL-10, or CD206 (Fig. 1H). These findings demonstrate that TSCC cell-derived exosomes promote M2-type polarization of macrophages.

3.2. M2-type macrophages infiltration in TSCC has a strong correlation with poor patient prognosis

To systematically investigate the prognostic impact of M2 macrophages in tongue squamous cell carcinoma (TSCC), we conducted bioinformatics analysis of 148 cases of TSCC and 15 cases of paracancerous tissues from the TCGA database. Using the ssGSEA algorithm, we evaluated the general state of immune cell infiltration (Fig. 2A). The results revealed that the M2-type macrophage infiltration fraction was significantly higher in TSCC tissues compared to paracancerous tissues (Fig. 2B).

After excluding samples with incomplete clinical data, we then performed correlation analysis between M2 macrophage markers and clinical parameters. A final cohort of 147 TSCC specimens was included for comprehensive clinicopathological analysis (Table 2). These 10 core M2 macrophage markers were used to establish a multivariate Cox regression model. We named the model "Iieb" (these 10 core M2 markers are involved in inflammation, immunity, extracellular matrix, and blood vascular related activities). Both risk factor correlation plots demonstrated significant survival differences between the high- and low-risk groups, consistent with the Kaplan-Meier (K-M) survival curves (Fig. 2C and D). The ROC curves demonstrated the robust predictive capacity of the model (Fig. 2E). In the univariate Cox regression, Iieb was identified as a key factor associated with increased prognostic risk (Fig. 2F). To eliminate potential interactions between factors, we conducted a multivariable Cox regression analysis, which confirmed that Iieb remained a significant factor associated with increased prognostic risk (Fig. 2G). Finally, we constructed a clinical nomogram incorporating these factors to predict patient outcomes (Fig. 2H).

To explore the possible mechanisms underlying the prognostic

impact of M2 macrophages in TSCC, we conducted differential gene expression and functional enrichment analyses. Volcano plot revealed a predominance of downregulated genes in the high-risk group compared to the low-risk group (Fig. S1A). Subsequent GO and KEGG enrichment analyses of these differentially expressed genes demonstrated significant enrichment in biological processes including multicellular organism development, phylogeny, and cellular developmental processes (Fig. S1B).

GO CC (Cellular component) analysis revealed significant enrichment in extracellular regions, endomembrane systems, and extracellular interstitial spaces (Fig. S1C). GO MF (Molecular function) analysis demonstrated enrichment in signaling receptor binding, carbohydrate derivative binding, and identical protein binding (Fig. S1D). KEGG analysis showed significant enrichment in cytokine receptor interaction, PI3K-AKT signaling pathway, focal adhesion, and MAPK signaling pathway (Fig. S1E). GSEA enrichment analysis showed that the differential genes inhibited the PI3K-AKT signaling pathway by suppressing BP: extracellular matrix organization, extracellular structural organization, and external encapsulating structure organization (Fig. S1F); CC: I-band, myofilament, and myonodule within rhabdomyosin protofibrils (Fig. S1G); MF: voltage-gated ion channel activation, voltage-gated channel activation, and extracellular matrix structural composition (Fig. S1H); KEGG: Th1 and Th2 cell differentiation, protein digestion and absorption, and cell adhesion molecules (Fig. S1I).

3.3. M2-type macrophage-conditioned medium promotes the proliferation, migration, and invasion of TSCC cells and protects these cells against cisplatin-induced apoptosis

To explore the functional impact of M2 macrophages on TSCC cell behavior, we cultured CAL27 and SCC9 cells with conditioned medium (CM) from exosome-induced M2-type macrophages. EdU results showed that M2-type macrophage-conditioned medium increased the proliferation of both CAL27 and SCC9 cells (Fig. 3A and B). Transwell analysis demonstrated that treatment with CM enhanced the invasive ability of both CAL27 and SCC9 cells (Fig. 3C and D). Scratch (wound healing) assay revealed that CM significantly promoted the migration ability of CAL27 and SCC9 cells (Fig. 3E and F). CAL27 and SCC9 tongue squamous cell carcinoma cells were treated with cisplatin at concentrations of 0, 1, 2, 4, and 8 μ M for 24, 48, and 72 h, respectively. Flow cytometry results indicated that the conditioned medium had a significant protective effect against cisplatin-induced apoptosis in CAL27 and SCC9 cells (Fig. 3G and H). In conclusion, these findings demonstrate that conditioned medium of M2-type macrophages derived from exosomes promotes proliferation, migration, and invasive ability of tongue cancer cells, and protects against cisplatin-induced apoptosis.

3.4. MiR-21-5p affects M2 macrophage polarization via regulating the ERK1/2 signaling pathway

Through small RNA sequencing of TSCC-derived exosomes, we identified 332 distinct miRNAs, among which miR-21-5p exhibited the highest expression levels in both CAL27 and SCC9 cell lines (Fig. 4A and B). MiR-21-5p was selected for subsequent studies. Subsequent KEGG signaling pathway enrichment analysis showed significant enrichment in the MAPK signaling pathway (Fig. 4C). A total of eight core target genes (RASGRP1, MYC, RPS6KA3, RASGRP3, NRAS, CHUK, HSPA8, GNG12) were identified by intersecting the genes enriched in the MAPK signaling pathway with the down-regulated genes among the M2 and M0-type macrophage differential genes in the GSE162698 dataset (Fig. 4D). Validation using the GSE124566 dataset (containing non-coding RNA-seq data from 10 TSCC specimens and 10 paracancerous tissues) confirmed significant overexpression of miR-21-5p in tumor tissues compared to normal counterparts (Fig. 4E–G).

Immunofluorescence was used to detect the uptake of GFP-labeled miR-21-5p mimics by M0 macrophages. Compared with control M0

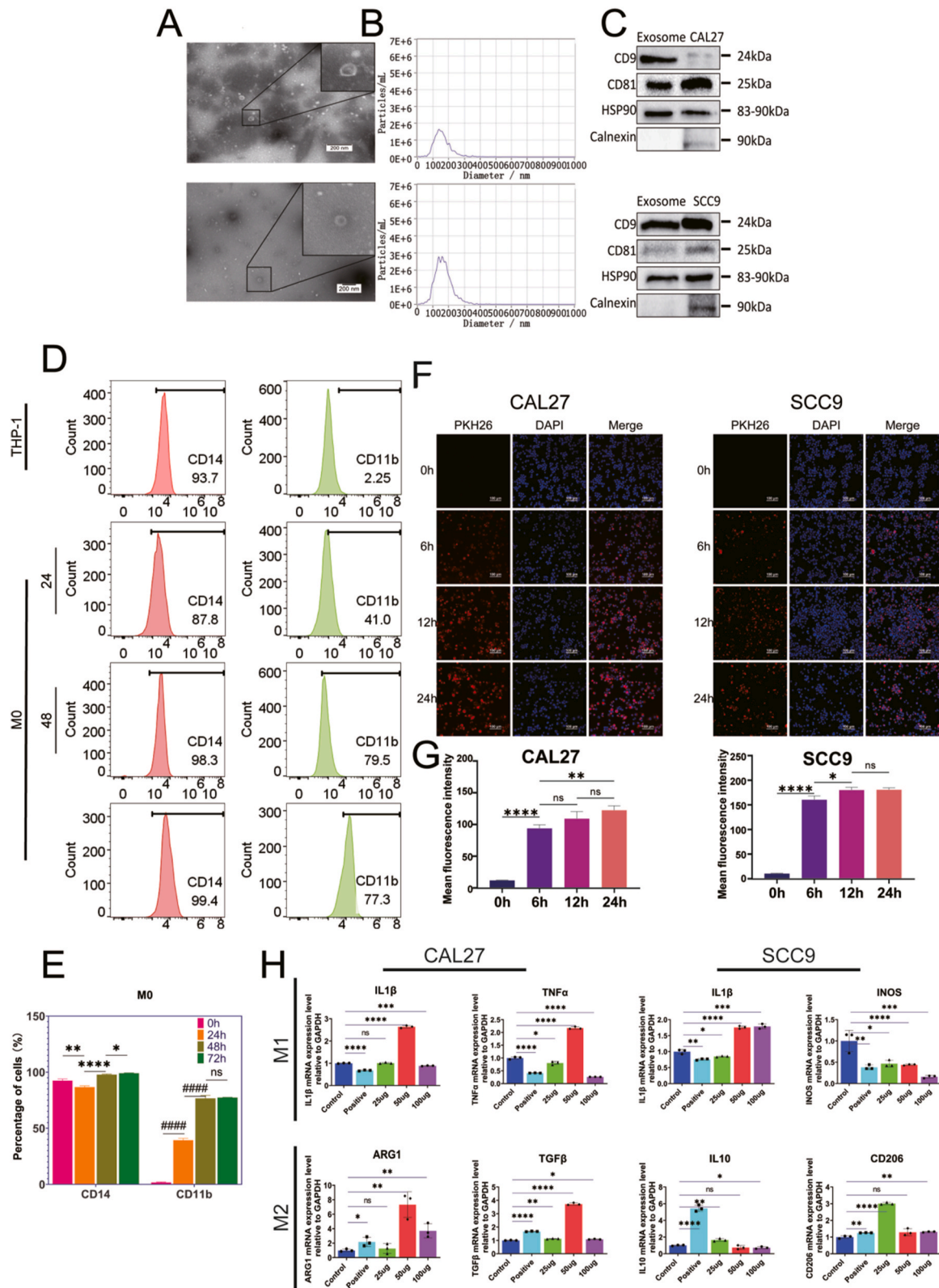


Fig. 1. Exosomes from TSCC cells promote M2-type polarization of TAMs. Under a transmission electron microscope, the exosomes from CAL27 and SCC9 cells exhibited a "cup-shaped" double membrane structure (A). Nanoparticle tracking analysis (NTA) of the exosomes showed that most were in the range of 30–150 nm in diameter, consistent with the size of exosomes (B). Western blot results showed positive expression of CD9, CD81, and HSP90, with negligible expression of Calnexin (C). Under the action of PMA, THP-1 cells had been successfully induced into M0-type macrophages (D–E). exosomes from CAL27 reached peak uptake after 12h, while those from SCC9 reached peak uptake after 6h (F–G). M0-type macrophages co-cultured with exosomes suppressed the expression of M1 makers encoding IL-1 β , TNF- α , or INOS, and increased the expression of M2 makers encoding Arg1, TGF- β , IL-10, or CD206 (H). (n = 3, ^{ns}p \geq 0.05, ^{*}p < 0.05, ^{**}/^{##}/^{###}/^{####}/^{#####}p < 0.01, ^{***}/^{####}/^{#####}p < 0.001, ^{****}/^{#####}p < 0.0001, nonparametric test).

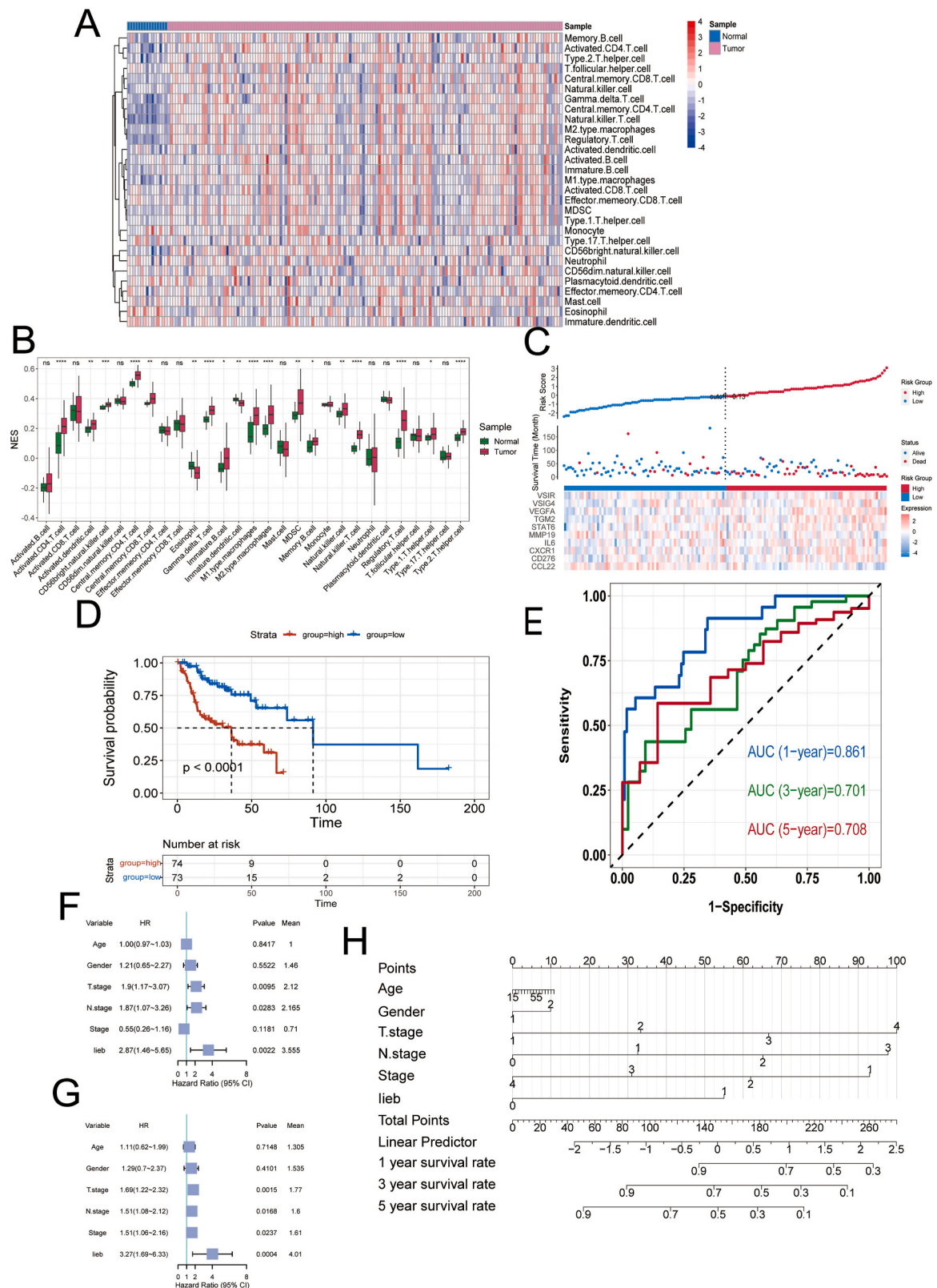


Fig. 2. M2-type macrophages infiltration in TSCC have a strong correlation with poor patient prognosis. ssGSEA algorithm was employed to evaluate the general state of immune cell infiltration (A). The results revealed that the M2-type macrophage infiltration fraction was significantly higher in tongue squamous carcinoma tissues compared to paracancerous tissues (B). Risk factor correlation plots showed significant survival differences between the high-risk and low-risk groups, consistent with the Kaplan-Meier (K-M) survival curves (C–D). The ROC curves demonstrated the model’s good predictive performance (E). In the univariate Cox regression, lieb was identified as a key factor associated with increased prognostic risk (F). To eliminate interactions between factors, we conducted a multivariable Cox regression analysis, which confirmed that lieb remained a significant factor associated with increased prognostic risk (G). Finally, we developed a nomogram model to clinically predict patients’ prognostic survival (H). (n = 3, ^{ns}p ≥ 0.05, *p < 0.05, **p < 0.01, ***p < 0.001, ****p < 0.0001, nonparametric test).

Table 2
Statistical table of clinical data for 147 patients with tongue squamous cell carcinoma.

	ALL N = 147	Alive N = 89	Dead N = 58	P.overall
Age	57.9(12.8)	57.5(13.2)	58.4(12.4)	0.659
Gender:				0.523
Female	45(30.6 %)	25(28.1 %)	20(34.5 %)	
Male	102(69.4 %)	64(71.9 %)	38(65.5 %)	
T_stage:				0.007
NA	3(2.04 %)	3(3.37 %)	0(0.00 %)	
T1	21(14.3 %)	16(18.0 %)	5(8.62 %)	
T2	49(33.3 %)	36(40.4 %)	13(22.4 %)	
T3	42(28.6 %)	19(21.3 %)	23(39.7 %)	
T4a	21(14.3 %)	8(8.99 %)	13(22.4 %)	
T4b	1(0.68 %)	1(1.12 %)	0(0.00 %)	
TX	10(6.80 %)	6(6.74 %)	4(6.90 %)	
N_stage:				0.035
NA	3(2.04 %)	3(3.37 %)	0(0.00 %)	
N0	52(35.4 %)	36(40.4 %)	16(27.6 %)	
N1	20(13.6 %)	16(18.0 %)	4(6.90 %)	
N2	3(2.04 %)	2(2.25 %)	1(1.72 %)	
N2a	2(1.36 %)	1(1.12 %)	1(1.72 %)	
N2b	38(25.9 %)	19(21.3 %)	19(32.8 %)	
N2c	10(6.80 %)	3(3.37 %)	7(12.1 %)	
N3	1(0.68 %)	0(0.00 %)	1(1.72 %)	
NX	18(12.2 %)	9(10.1 %)	9(15.5 %)	
M_stage:				0.167
NA	81(55.1 %)	44(49.4 %)	37(63.8 %)	
M0	49(33.3 %)	32(36.0 %)	17(29.3 %)	
MX	17(11.6 %)	13(14.6 %)	4(6.90 %)	
Stage:				0.258
NA	17(11.6 %)	10(11.2 %)	7(12.1 %)	
StageI	13(8.84 %)	10(11.2 %)	3(5.17 %)	
StageII	22(15.0 %)	16(18.0 %)	6(10.3 %)	
StageIII	33(22.4 %)	22(24.7 %)	11(19.0 %)	
StageIVA	60(40.8 %)	30(33.7 %)	30(51.7 %)	
StageIVB	2(1.36 %)	1(1.12 %)	1(1.72 %)	
lieb:				0.001
High	74(50.3 %)	34(38.2 %)	40(69.0 %)	
Low	73(49.7 %)	55(61.8 %)	18(31.0 %)	

TSCC patients' clinical data, excluding samples with incomplete clinical data, resulting in 147 samples.

macrophages, experimental M0 macrophages significantly uptook miR-21-5p (Fig. 5A and B). Western blotting was used to detect the expression of key molecules in the MAPK signaling pathway. The results showed that compared with the control group (M0 macrophages), the experimental group (M0+miR-21-5p) had a significantly decreased expression level of p-ERK1/2, while the expression levels of p-JNK and p-P38 were unchanged or increased (Fig. 5C). The expression of ARG1 was significantly elevated. Additionally, in the presence of the ERK1/2 agonist HY-W010970, the ARG1 expression levels were reduced compared to the experimental group (M0+miR-21-5p) (Fig. 5D).

4. Discussion

In the TSCC tumor microenvironment, miR-21-5p secreted by cancer cells is delivered to macrophages via exosomes, prompting the latter to polarize into M2-type macrophages, a process closely related to the ERK1/2 signaling pathway. Our ssGSEA analysis of transcriptomic data from the TCGA database further confirmed that the enrichment scores of M2-type macrophages are significantly elevated in TSCC tissues compared to paracancerous tissues. These findings suggest a progressive accumulation of M2-type macrophages during TSCC tumorigenesis. Functionally, these M2-polarized macrophages enhance TSCC malignancy by promoting proliferative capacity, invasive potential, migratory activity, and apoptotic resistance. Overall, miR-21-5p, an miRNA from TSCC cell-derived exosomes, is involved in the polarization of TAMs. This study provides new insights into the intercellular communication between TSCC cells and macrophages.

Our experimental results confirmed that exosomes derived from TSCC cells can promote M2 polarization of TAMs, which is consistent with the current majority of reported views [21–23]. Although M1 and M2 macrophage polarization is defined by distinct molecular markers, the exact markers may differ among studies due to variations in cell sources or stimulation protocols [24–26]. Based on established literature, we selected five canonical M1 macrophage markers (IL-1 β , TNF- α , iNOS, CD86, and IL-6) and five M2 macrophage markers (IL-10, CD163, CD206, TGF- β , and ARG1) for evaluation [27–29]. Due to variations in cellular origin and experimental interventions, part of the evaluated polarization markers did not show statistically significant differences between CAL27 and SCC9 cell lines. Therefore, we focused our presentation on these significantly altered markers (Fig. 1H), while omitting those that did not reach statistical significance in our experimental system. The distinct M1- and M2-type macrophage markers identified in CAL27 and SCC9 cell lines, combined with the differential exosome-mediated induction efficiencies of M0 macrophage polarization observed in this study, collectively demonstrate substantial heterogeneity within the TSCC tumor microenvironment [30,31]. Upon induction of M0-type macrophages, the presence of CAL27 exosomes (100 μ g) led to decreased expression levels of M1-type macrophage markers (IL1 β , TNF α), while increasing the expression levels of M2-type macrophage markers (ARG1, TGF β). By contrast, in the presence of SCC9 exosomes (25 μ g), the expression levels of M1-type macrophage markers (IL1 β , INOS) were decreased, while those of M2-type macrophage markers (IL10, CD206) were increased.

Cox regression modeling, also known as "proportional risk regression modeling", is a classic clinical prediction model commonly employed in studies related to biomarkers and factors affecting prognostic survival time [32–35]. Multifactorial Cox regression modeling enhances model accuracy by considering multiple factors and reducing interference from unconsidered factors compared to single-factor analysis [36]. In this study, a multifactorial Cox regression model was constructed incorporating the 10 core genes selected by Lasso regression. Samples were scored based on the Hazard Ratio, categorizing them into high-risk and low-risk groups based on the median scores for survival time prediction. ROC curve analysis revealed that our constructed model demonstrated relatively good performance in predicting patients' 1-, 3-, and 5-year survival rates. Single and multifactorial Cox regression analyses highlighted the significance of the Lieb model we constructed as an important factor increasing prognostic risk in patients with tongue squamous carcinoma. We constructed a nomogram model to predict patient prognostic survival rates. Interestingly, while clinical staging typically exhibits a positive correlation with patient outcomes, the nomogram column line graph depicted a negative correlation. This discrepancy may stem from significant missing data (55.1 %) regarding metastatic status (M stage) in the TNM staging system, potentially compromising staging accuracy and subsequent survival predictions. These findings underscore the need for more comprehensive clinical datasets to facilitate robust prognostic analyses.

Previous studies have demonstrated a link between the inhibition of MAPK and ERK1/2 signaling pathways and the polarization of M2-type macrophages. In non-tumor diseases, reduced ERK expression typically promotes M2-type macrophage polarization. For instance, Zhou et al. have reported that Tectoridin, a potent isoflavone with anti-inflammatory properties, induces macrophage M2 polarization. Tectoridin could potentially treat severe acute pancreatitis by inhibiting the ERK and MAPK signaling pathways [37]. In ulcerative colitis (UC), flavopiridol (COP) inhibits mitogen-activated protein kinase (MEK) or extracellularly regulated protein kinase (ERK) signaling pathways, thereby inhibiting macrophage M1 polarization. Conversely, COP increases the expression of CCAAT enhancer-binding protein β , promoting macrophage M2 polarization [38]. Similarly, Chen et al. have demonstrated that carvacrol inhibits MAPK signaling molecules P-JNK, P-ERK, and P-P38, reducing inflammatory mediator production and promoting M2-type macrophage polarization [39]. In tumor microenvironments,

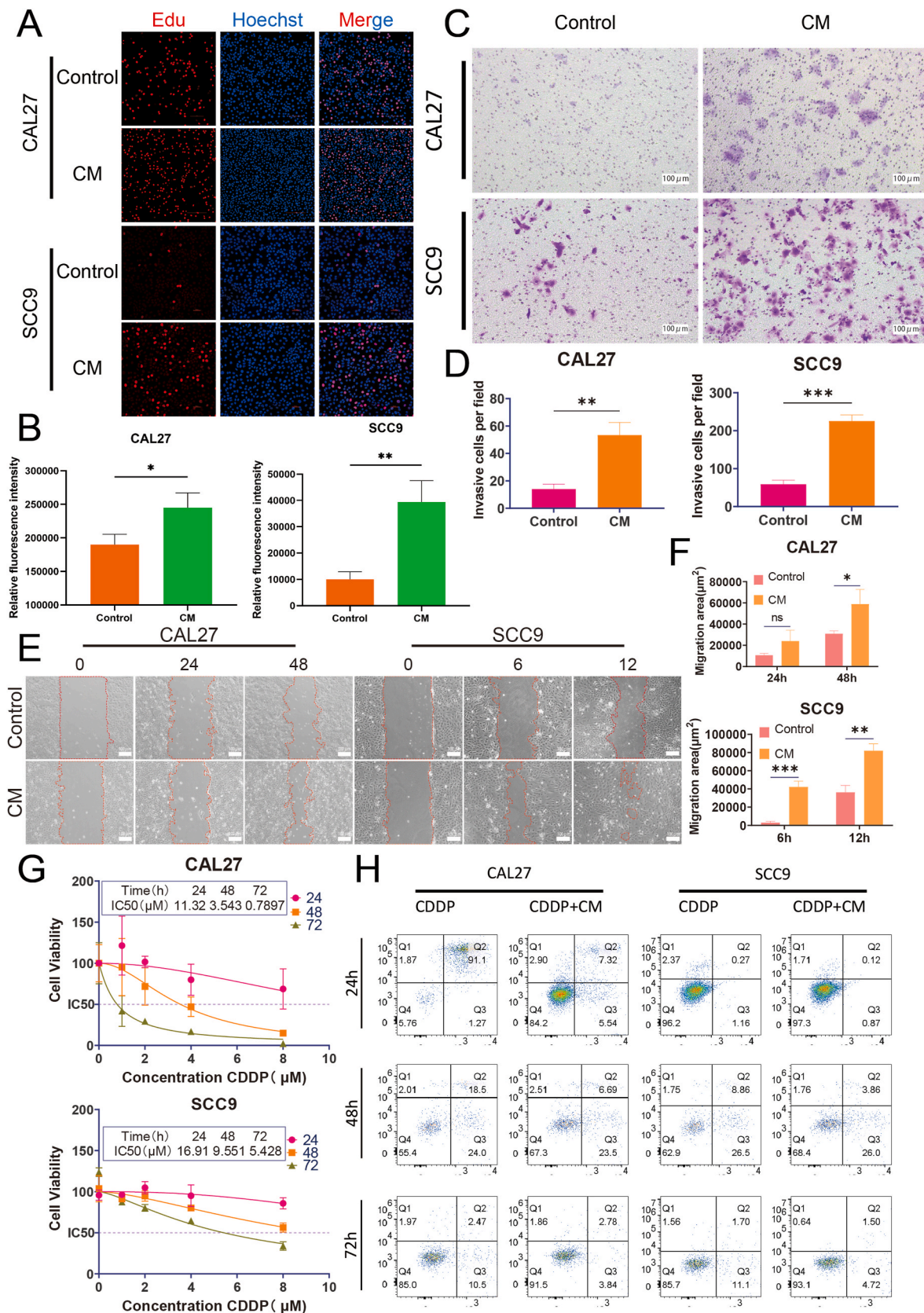


Fig. 3. M2-type macrophage-conditioned medium promotes the proliferation, migration, and invasion of TSCC cells and protects these cells against cisplatin-induced apoptosis. EdU results showed that M2-type macrophage conditioned medium increased the proliferation of both CAL27 and SCC9 cells (A–B). Transwell analysis demonstrated that treatment with CM enhanced the invasive ability of both CAL27 and SCC9 cells (C–D). Scratch assay revealed that CM significantly promoted the migration ability of CAL27 and SCC9 cells (E–F). Flow cytometry results indicated that the conditioned medium had a significant protective effect against cisplatin-induced apoptosis in CAL27 and SCC9 cells (G–H). (n = 3, ^{ns}p ≥ 0.05, *p < 0.05, **p < 0.01, ***p < 0.001, nonparametric test).

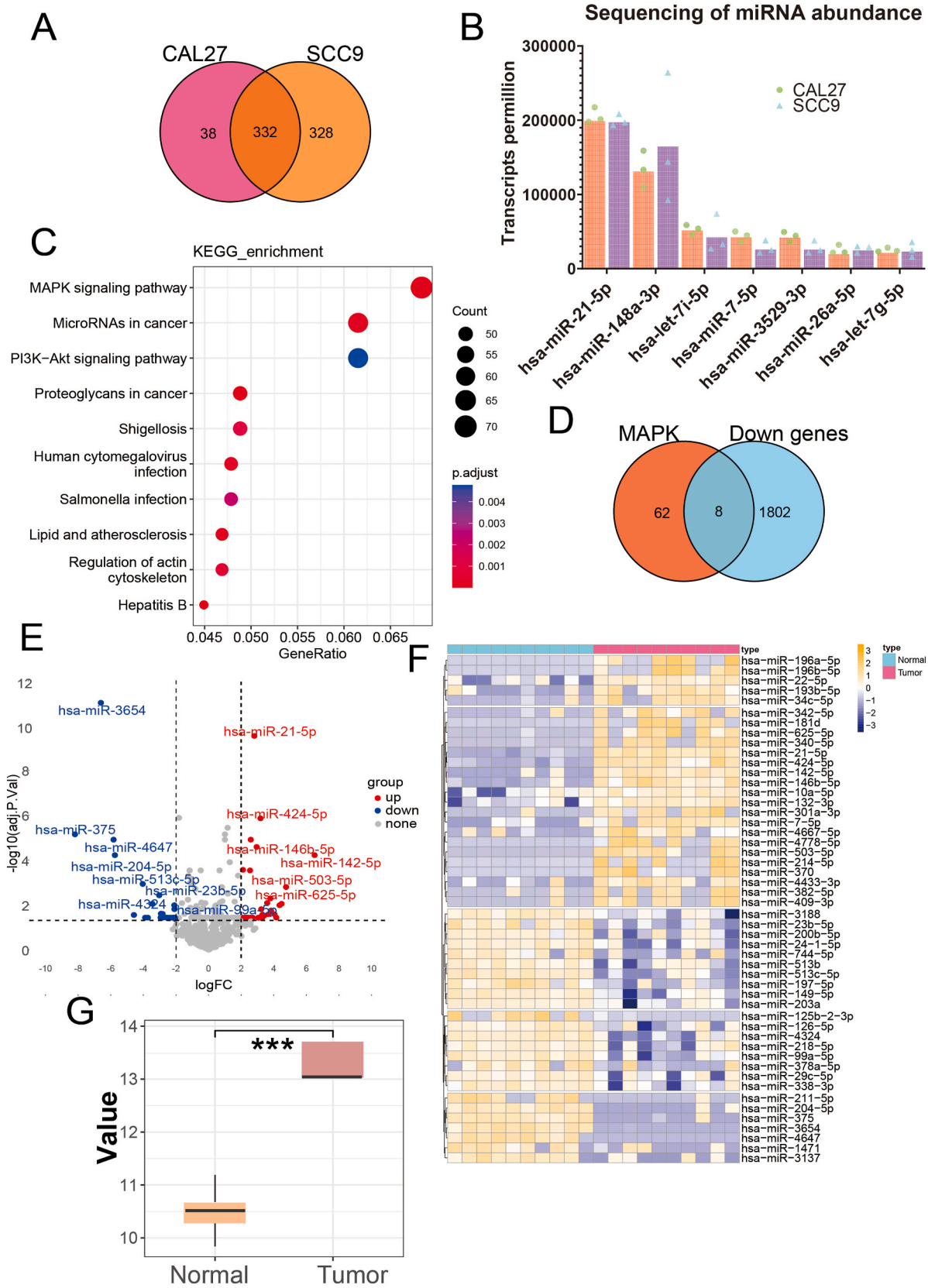


Fig. 4. MiR-21-5p affects M2 macrophage polarization via regulating the ERK1/2 signaling pathway. There were a total of 332 miRNAs in the exosomes of CAL27 and SCC9, with miR-21-5p ranking first (A–B). KEGG signaling pathway enrichment analysis showed significant enrichment of the MAPK signaling pathway (C). A total of eight core target genes (RASGRP1, MYC, RPS6KA3, RASGRP3, NRAS, CHUK, HSPA8, GNG12) were identified by intersecting the genes enriched in the MAPK signaling pathway with the down-regulated genes among the M2 and M0-type macrophage differential genes in the GSE162698 dataset (D). We analyzed the GSE124566 dataset, miR-21-5p was highly expressed in tongue squamous carcinoma tissues compared to paracancerous tissues (E–G).

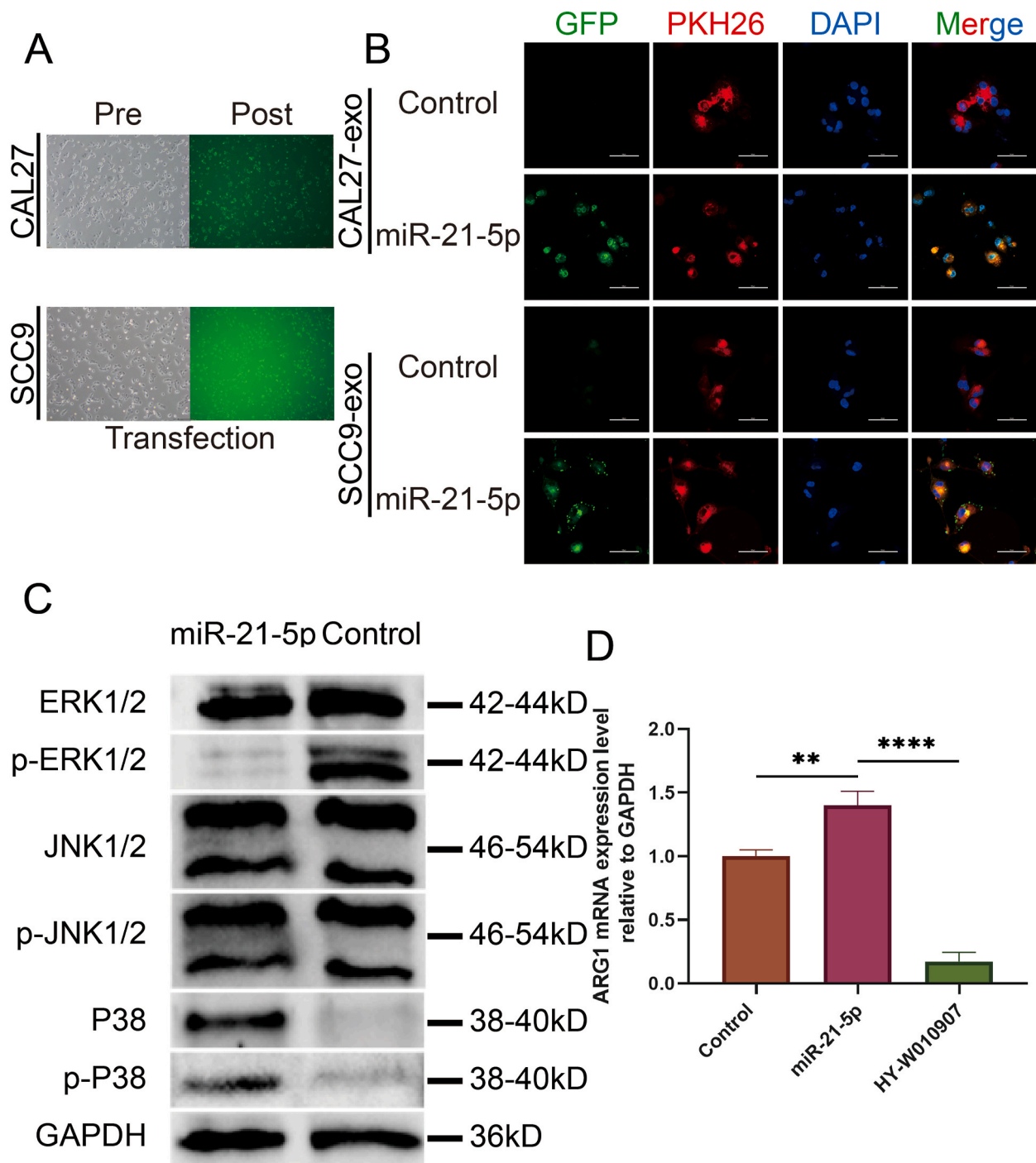


Fig. 5. MiR-21-5p affects M2 macrophage polarization via regulating the ERK1/2 signaling pathway. Compared with control M0 macrophages, experimental M0 macrophages significantly uptook miR-21-5p (A–B). The results showed that compared with the control group (M0 macrophages), the experimental group (M0+miR-21-5p) had a significantly decreased expression level of p-ERK1/2, while the expression levels of p-JNK and p-P38 were unchanged or increased (C). The expression of ARG1 was significantly elevated. Additionally, in the presence of the ERK1/2 agonist HY-W010970, the ARG1 expression levels were reduced compared to the experimental group (M0+miR-21-5p) (D). (n = 3, ^{ns}p ≥ 0.05, *p < 0.05, **p < 0.01, ***p < 0.001, nonparametric test).

M2-type macrophage polarization is frequently associated with decreased p-ERK1/2 levels. For example, coagulation factor X (FX) promotes M2 subtype macrophage polarization and accelerates glioblastoma multiforme growth by binding to extracellular signaling-associated kinase (ERK) 1/2 and inhibiting p-ERK1/2 in GBM cells [40]. Conversely, the activation of the ERK1/2 signaling pathway is typically associated with M1-type macrophage polarization. Peter et al. found that C1q/TNF-related protein family member C1qtnf3 inhibits macrophage accumulation in tumor-associated inguinal adipose tissue

by stimulating the ERK and Akt pathways, leading to increased M1-like polarization and promoting M1-type macrophage polarization [41].

Sequencing analysis identified miR-21-5p as the most highly expressed miRNA in exosomes derived from both CAL27 and SCC9 TSCC cell lines, implicating its potential functional importance in intercellular communication within the tumor microenvironment. Pathway enrichment analysis indicated a significant enrichment of the MAPK signaling pathway, suggesting that miR-21-5p may influence cellular communication by modulating this pathway (specifically ERK1/2, JNK, or P38

MAPK) in target cells. Further experiments revealed that miR-21-5p promotes M2 polarization of TAMs by inhibiting phosphorylation of ERK1/2. Interestingly, the Control group exhibited low expression levels of both P38 and p-P38, with minimal protein bands. These findings suggest that PMA induction may suppress the P38 or p-P38 expression in M0-type macrophages. However, additional experimental validation is required to conclusively determine the effects of PMA induction on P38/p-P38 expression levels in M0 macrophages.

A major limitation of this study is that we referred to previous literature and only detected the expression change of M1 and M2 macrophage markers at the mRNA level, without detecting proteins. In response to this shortcoming, we will continuously improve in future research in order to make greater contributions to the treatment of TSCC.

5. Conclusion

The mechanisms driving M2-polarized tumor-associated macrophages in TSCC and their impact on tumor behavior and prognosis remain unclear. In this study, we constructed a miR-21-5p-mediated cellular interaction model between tongue squamous carcinoma cells and M2-type macrophages (Fig. 6). Our findings demonstrate that exosomes serve as carriers for delivering miR-21-5p from tongue squamous carcinoma cells to macrophages, thereby influencing tumor progression by promoting macrophage M2-type polarization. Therefore, targeting miR-21-5p within tongue squamous carcinoma exosomes may represent a potential therapeutic strategy for treating tongue squamous carcinoma. Modulating miR-21-5p levels to reduce M2-type macrophage polarization and consequently impede tumor progression could emerge as a viable treatment option for tongue squamous carcinoma in the

future.

CRedit authorship contribution statement

Zixian Xu: Writing – original draft, Visualization, Validation, Software, Investigation, Formal analysis, Conceptualization. **Xin Fang:** Validation, Software, Investigation, Formal analysis. **Shan Wang:** Validation, Software, Investigation, Formal analysis. **Jiabei Mu:** Visualization, Validation, Software, Formal analysis. **Qixian Gai:** Visualization, Validation, Software, Formal analysis. **Yantong Chen:** Visualization, Validation, Software, Formal analysis. **Zheyi Sun:** Writing – review & editing, Supervision, Methodology, Data curation, Conceptualization. **Jiemei Zhai:** Writing – review & editing, Supervision, Resources, Project administration, Methodology, Funding acquisition.

Data availability statement

The data involved in this study comes from the public database TCGA or self sequencing data. If necessary, we can provide it.

Ethics approval statement

Ethical approval to report this case was obtained from the Medical Ethics Committee of the Affiliated Stomatological Hospital of Kunming Medical University (KYKQ2022MEC0098).

Funding statement

This work was supported by the National Natural Science Foundation

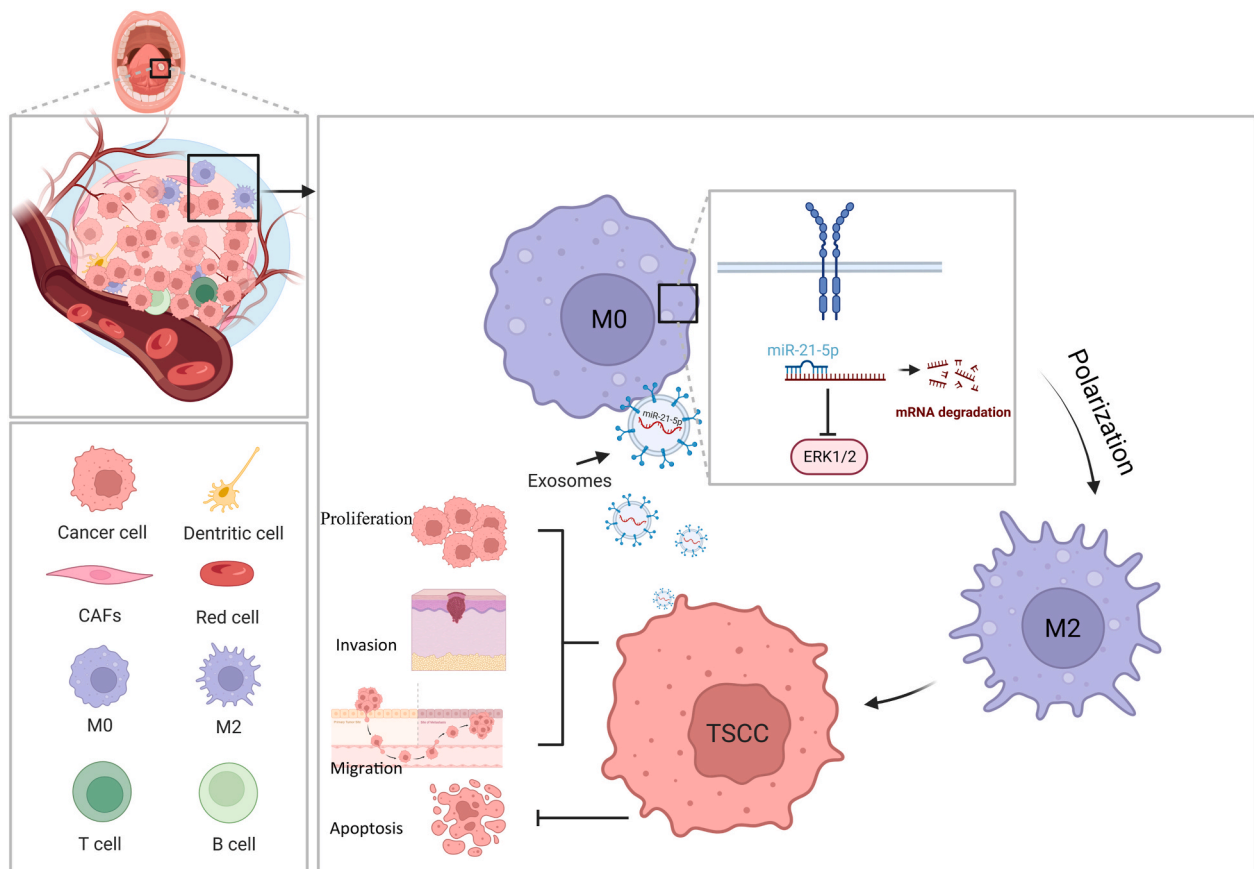


Fig. 6. Tongue squamous cell carcinoma (TSCC) cell-derived exosomes exhibit elevated miR-21-5p levels. Upon internalization by M0 macrophages, exosomal miR-21-5p suppresses ERK1/2 signaling pathway, thereby driving M2 polarization. These M2-macrophages then critically enhance TSCC cell proliferation, invasion, and migration while suppressing their response to cisplatin-induced apoptosis.

of China (Grant No. 81960203) and the Reserve Talents for Academic and Technical Leaders of Middle-aged and Young People in Yunnan Province (Grant No. 202305AC160001).

Declaration of competing interest

The authors declare that they have no known competing financial interests or personal relationships that could have appeared to influence the work reported in this paper.

Acknowledgements

We would like to thank the Yunnan Provincial Key Laboratory of Oral Medicine for providing the experimental platform.

Appendix A. Supplementary data

Supplementary data to this article can be found online at <https://doi.org/10.1016/j.ncrna.2025.05.006>.

References

- [1] K. Rusthoven, A. Ballonoff, D. Raben, C. Chen, Poor prognosis in patients with stage I and II oral tongue squamous cell carcinoma, *Cancer* 112 (2008) 345–351, <https://doi.org/10.1002/ncr.23183>.
- [2] M. Ogawa, S. Yokoo, T. Yamaguchi, K. Suzuki, M. Seki, T. Shimizu, T. Makiguchi, Treatment strategy for cervical lymph node metastases from early-stage tongue and floor of the mouth squamous cell carcinoma using tumour budding and depth of invasion as predictors, *Clin. Oral Invest.* 28 (2024) 580, <https://doi.org/10.1007/s00784-024-05974-y>.
- [3] K. Matsuo, J. Akiba, J. Kusukawa, H. Yano, Squamous cell carcinoma of the tongue: subtypes and morphological features affecting prognosis, *Am. J. Physiol. Cell Physiol.* 323 (2022) C1611–C1623, <https://doi.org/10.1152/ajpcell.00098.2022>.
- [4] A. Elseragy, I.O. Bello, A. Wahab, R.D. Coletta, A.A. Mäkitie, I. Leivo, A. Almagush, T. Salo, Emerging histopathologic markers in early-stage oral tongue cancer: a systematic review and meta-analysis, *Head Neck* 44 (2022) 1481–1491, <https://doi.org/10.1002/hed.27022>.
- [5] B. Toledo, L. Zhu Chen, M. Paniagua-Sancho, J.A. Marchal, M. Perán, E. Giovannetti, Deciphering the performance of macrophages in tumour microenvironment: a call for precision immunotherapy, *J. Hematol. Oncol.* 17 (2024) 44, <https://doi.org/10.1186/s13045-024-01559-0>.
- [6] S. Han, W. Wang, S. Wang, T. Yang, G. Zhang, D. Wang, R. Ju, Y. Lu, H. Wang, L. Wang, Tumor microenvironment remodeling and tumor therapy based on M2-like tumor associated macrophage-targeting nano-complexes, *Theranostics* 11 (2021) 2892–2916, <https://doi.org/10.7150/thno.50928>.
- [7] W. Kuo, J. Chang, C. Chen, N. Tsao, C. Chang, Autophagy drives plasticity and functional polarization of tumor-associated macrophages, *IUBMB Life* 74 (2022) 157–169, <https://doi.org/10.1002/iub.2543>.
- [8] W. Zhou, S.Q. Ke, Z. Huang, W. Flavahan, X. Fang, J. Paul, L. Wu, A.E. Sloan, R. E. McLendon, X. Li, J.N. Rich, S. Bao, Periostin secreted by glioblastoma stem cells recruits M2 tumour-associated macrophages and promotes malignant growth, *Nat. Cell Biol.* 17 (2015) 170–182, <https://doi.org/10.1038/ncb3090>.
- [9] P. Laskar Pranav, M. Jaggi, S.C. Chauhan, M.M. Yallapu, Biomolecule-functionalized nanoformulations for prostate cancer theranostics, *J. Adv. Res.* 51 (2023) 197–217, <https://doi.org/10.1016/j.jare.2022.11.001>.
- [10] G. Yang, J. Qiu, J. Xu, G. Xiong, F. Zhao, Z. Cao, G. Chen, Y. Liu, J. Tao, L. Zheng, L. Wang, R. Qin, T. Zhang, Using a microRNA panel of circulating exosomes for diagnosis of pancreatic cancer: multicentre case-control study, *Br. J. Surg.* 110 (2023) 908–912, <https://doi.org/10.1093/bjs/znac375>.
- [11] Y. Song, Y. You, X. Xu, J. Lu, X. Huang, J. Zhang, L. Zhu, J. Hu, X. Wu, X. Xu, W. Tan, Y. Du, Adipose-derived mesenchymal stem cell-derived exosomes biopotentiates extracellular matrix hydrogels accelerate diabetic wound healing and skin regeneration, *Adv. Sci.* 10 (2023) 2304023, <https://doi.org/10.1002/adv.202304023>.
- [12] F. Teng, M. Fussenegger, Shedding light on extracellular vesicle biogenesis and bioengineering, *Adv. Sci.* 8 (2021) 2003505, <https://doi.org/10.1002/adv.202003505>.
- [13] X. Chen, O. Rechavi, Plant and animal small RNA communications between cells and organisms, *Nat. Rev. Mol. Cell Biol.* 23 (2022) 185–203, <https://doi.org/10.1038/s41580-021-00425-y>.
- [14] L. Zhang, K. Zhang, J. Zhang, J. Zhu, Q. Xi, H. Wang, Z. Zhang, Y. Cheng, G. Yang, H. Liu, X. Guo, D. Zhou, Z. Xue, Y. Li, Q. Zhang, Y. Da, L. Liu, Z. Yin, Z. Yao, R. Zhang, Loss of fragile site-associated tumor suppressor promotes antitumor immunity via macrophage polarization, *Nat. Commun.* 12 (2021) 4300, <https://doi.org/10.1038/s41467-021-24610-x>.
- [15] N.R. Anderson, N.G. Minutolo, S. Gill, M. Klichinsky, Macrophage-based approaches for cancer immunotherapy, *Cancer Res.* 81 (2021) 1201–1208, <https://doi.org/10.1158/0008-5472.CAN-20-2990>.
- [16] S.K. Biswas, P. Allavena, A. Mantovani, Tumor-associated macrophages: functional diversity, clinical significance, and open questions, *Semin. Immunopathol.* 35 (2013) 585–600, <https://doi.org/10.1007/s00281-013-0367-7>.
- [17] J. Chen, K. Zhang, Y. Zhi, Y. Wu, B. Chen, J. Bai, X. Wang, Tumor-derived exosomal miR-19b-3p facilitates M2 macrophage polarization and exosomal LINC00273 secretion to promote lung adenocarcinoma metastasis via Hippo pathway, *Clin. Transl. Med.* 11 (2021) e478, <https://doi.org/10.1002/ctm2.478>.
- [18] S. Qiu, L. Xie, C. Lu, C. Gu, Y. Xia, J. Lv, Z. Xuan, L. Fang, J. Yang, L. Zhang, Z. Li, W. Wang, H. Xu, B. Li, Z. Xu, Gastric cancer-derived exosomal miR-519a-3p promotes liver metastasis by inducing intrahepatic M2-like macrophage-mediated angiogenesis, *J. Exp. Clin. Cancer Res.* 41 (2022) 296, <https://doi.org/10.1186/s13046-022-02499-8>.
- [19] H. Zongqiang, C. Jiapeng, Z. Yingpeng, Y. Chuntao, W. Yiting, Z. Jiashun, L. Li, Exosomal miR-452-5p induce M2 macrophage polarization to accelerate hepatocellular carcinoma progression by targeting TIMP3, *J. Immunol. Res.* 2022 (2022) 1032106, <https://doi.org/10.1155/2022/1032106>.
- [20] Y. Guo, J. Cui, X. Liang, T. Chen, C. Lu, T. Peng, Pancreatic cancer stem cell-derived exosomal miR-210 mediates macrophage M2 polarization and promotes gemcitabine resistance by inducing intrahepatic M2-like macrophage-mediated angiogenesis, *Int. Immunopharmacol.* 127 (2024) 111407, <https://doi.org/10.1016/j.intimp.2023.111407>.
- [21] Z. Wang, S.Y. Kim, W. Tu, J. Kim, A. Xu, Y.M. Yang, M. Matsuda, L. Reoliz, T. Tsuchiya, S. Billet, A. Gangi, M. Noureddin, B.A. Falk, S. Kim, W. Fan, M. Tighiouart, S. You, M.S. Lewis, S.J. Pandol, D. Di Vizio, A. Merchant, E. M. Posadas, N.A. Bhowmick, S.C. Lu, E. Seki, Extracellular vesicles in fatty liver promote a metastatic tumor microenvironment, *Cell Metab.* 35 (2023) 1209–1226. e13, <https://doi.org/10.1016/j.cmet.2023.04.013>.
- [22] L. Xu, W. Li, D. Liu, J. Cao, J. Ge, X. Liu, Y. Wang, Y. Teng, P. Liu, X. Guo, C. He, M. Liu, L. Tian, ANXA3-Rich exosomes derived from tumor-associated macrophages regulate ferroptosis and lymphatic metastasis of laryngeal squamous cell carcinoma, *Cancer Immunol. Res.* 12 (2024) 614–630, <https://doi.org/10.1158/2326-6066.CIR-23-095>.
- [23] S. Du, J. Qian, S. Tan, W. Li, P. Liu, J. Zhao, Y. Zeng, L. Xu, Z. Wang, J. Cai, Tumor cell-derived exosomes deliver TIE2 protein to macrophages to promote angiogenesis in cervical cancer, *Cancer Lett.* 529 (2022) 168–179, <https://doi.org/10.1016/j.canlet.2022.01.005>.
- [24] N. Tan, G. Jian, J. Peng, X. Tian, B. Chen, Chishao - fuzi herbal pair restore the macrophage M1/M2 balance in acute-on-chronic liver failure, *J. Ethnopharmacol.* 328 (2024) 118010, <https://doi.org/10.1016/j.jep.2024.118010>.
- [25] L. Yi, Y. Chen, Y. Zhang, H. Huang, J. Li, Y. Qu, T. Wang, J. Chai, Deleting fibroblast growth factor 2 in macrophages aggravates septic acute lung injury by increasing M1 polarization and inflammatory cytokine secretion, *Mol Biomed* 5 (2024) 50, <https://doi.org/10.1186/s43556-024-00203-0>.
- [26] L. Shen, L. Kang, D. Wang, J. Xun, C. Chen, L. Du, M. Zhang, J. Gong, X. Mi, S. Yue, Y. Zhang, X. Song, R. Xiang, Z. Zhang, X. Tan, Legumain-deficient macrophages promote senescence of tumor cells by sustaining JAK1/STAT1 activation, *Cancer Lett.* 472 (2020) 40–49, <https://doi.org/10.1016/j.canlet.2019.12.013>.
- [27] J.-N. Song, K. Liu, J. Mei, L. Wang, J. Lin, P. Du, Y.-C. Liu, Y. Wan, R.C.B. Wong, J.-Y. Yin, P.-Y. Wang, Defined surface physicochemical cues inhibit M1 polarization of human macrophages using colloidal self-assembled patterns, *ACS Appl. Mater. Interfaces* 15 (2023) 35832–35846, <https://doi.org/10.1021/acsaami.3c04692>.
- [28] J. Song, D. Peng, Y. Peng, G. Zhao, Y. Ren, L. Guo, L. Ren, X. Zhang, X. Xie, Y. Zhang, L. Cao, Y. Li, The new pattern for dual NOTCH pathway involving nuclear transcription and mitochondrial regulation supports therapeutic mechanism of 4-butyl benzophenone derivatives against SIRS, *Free Radic. Biol. Med.* 223 (2024) 306–324, <https://doi.org/10.1016/j.freeradbiomed.2024.07.036>.
- [29] J.R. Nakkala, Y. Duan, J. Ding, W. Muhammad, D. Zhang, Z. Mao, H. Ouyang, C. Gao, Macrophage membrane-functionalized nanofibrous mats and their immunomodulatory effects on macrophage polarization, *Acta Biomater.* 141 (2022) 24–38, <https://doi.org/10.1016/j.actbio.2021.12.026>.
- [30] S. Fan, H. Zheng, Y. Zhan, J. Luo, H. Zang, H. Wang, W. Wang, Y. Xu, Somatostatin receptor2 (SSTR2) expression, prognostic implications, modifications and potential therapeutic strategies associates with head and neck squamous cell carcinomas, *Crit. Rev. Oncol. Hematol.* 193 (2024) 104223, <https://doi.org/10.1016/j.critrevonc.2023.104223>.
- [31] P. Parashar Antra, H. Hungyo, A. Jain, S. Ahmad, V. Tandon, Unraveling molecular mechanisms of head and neck cancer, *Crit. Rev. Oncol. Hematol.* 178 (2022) 103778, <https://doi.org/10.1016/j.critrevonc.2022.103778>.
- [32] X. Wu, X. Feng, Y. He, Y. Gao, S. Yang, Z. Shao, C. Yang, H. Wang, Z. Ye, IL-4 administration exerts preventive effects via suppression of underlying inflammation and TNF- α -induced apoptosis in steroid-induced osteonecrosis, *Osteoporos. Int.* 27 (2016) 1827–1837, <https://doi.org/10.1007/s00198-015-3474-6>.
- [33] E.X. Chen, J.M. Loree, E. Titmuss, D.J. Jonker, H.F. Kennecke, S. Berry, F. Couture, C.E. Ahmad, J.R. Goffin, P. Kavan, M. Harb, B. Colwell, S. Samimi, B. Samson, T. Abbas, N. Aucoin, F. Aubin, S. Koski, A.C. Wei, D. Tu, C.J. O’Callaghan, Liver metastases and immune checkpoint inhibitor efficacy in patients with refractory metastatic colorectal cancer: a secondary analysis of a randomized clinical trial, *JAMA Netw. Open* 6 (2023) e2346094, <https://doi.org/10.1001/jamanetworkopen.2023.46094>.
- [34] W. Huang, W. Xiong, L. Tang, C. Chen, Q. Yuan, C. Zhang, K. Zhou, Z. Sun, T. Zhang, Z. Han, H. Feng, X. Liang, Y. Zhong, H. Deng, L. Yu, Y. Xu, W. Wang, L. Shen, G. Li, Y. Jiang, Non-invasive CT imaging biomarker to predict immunotherapy response in gastric cancer: a multicenter study, *J. Immunother. Cancer* 11 (2023) e007807, <https://doi.org/10.1136/jitc-2023-007807>.

- [35] K. Kluge, H. Einspieler, D. Haberl, C. Spielvogel, S. Stoiber, C. Vranka, L. Papp, S. Wunsch, G. Egger, G. Kramer, B. Grubmüller, S. Shariat, M. Hacker, L. Kenner, A. Haug, Examining the relationship and prognostic significance of cell-free DNA levels and the PSMA-positive tumor volume in men with prostate cancer: a retrospective–prospective [68 Ga]Ga-PSMA-11 PET/CT study, *J. Nucl. Med.* 65 (2024) 63–70, <https://doi.org/10.2967/jnumed.123.266158>.
- [36] Z. Wang, Y. Liu, L. Wei, J.S. Ji, Y. Liu, R. Liu, Y. Zha, X. Chang, L. Zhang, Q. Liu, Y. Zhang, J. Zeng, T. Dong, X. Xu, L. Zhou, J. He, Y. Deng, B. Zhong, X. Wu, What are the risk factors of hospital length of stay in the novel coronavirus pneumonia (COVID-19) patients? A survival analysis in southwest China, *PLoS One* 17 (2022) e0261216, <https://doi.org/10.1371/journal.pone.0261216>.
- [37] L. Zhou, J. Yu, S. Wang, Y. Ma, X. Liu, X. Zhang, Y. Luo, S. Wen, L. Li, W. Li, X. Niu, Tectoridin alleviates caerulein-induced severe acute pancreatitis by targeting ERK2 to promote macrophage M2 polarization, *Arch. Biochem. Biophys.* 752 (2024) 109873, <https://doi.org/10.1016/j.abb.2023.109873>.
- [38] M. Zhao, P. Li, D. Qiao, S. Hua, Q. Yue, Y. Dai, Y. Huang, J. Jiang, H. Yin, M. Li, Y. Ding, X. Yang, Y. Ma, K. Ding, L. Zeng, N6-methyladenosine modification of TSC1 mRNA contributes to macrophage polarization regulated by Coptisine in DSS-induced ulcerative colitis, *Phytomedicine* 122 (2024) 155153, <https://doi.org/10.1016/j.phymed.2023.155153>.
- [39] S. Chen, H. Xu, Y. He, C. Meng, Y. Fan, Y. Qu, Y. Wang, W. Zhou, X. Huang, H. You, Carveol alleviates osteoarthritis progression by acting on synovial macrophage polarization transformation: an in vitro and in vivo study, *Chem. Biol. Interact.* 387 (2024) 110781, <https://doi.org/10.1016/j.cbi.2023.110781>.
- [40] Y. Zhang, J. Feng, H. Fu, C. Liu, Z. Yu, Y. Sun, X. She, P. Li, C. Zhao, Y. Liu, T. Liu, Q. Liu, Q. Liu, G. Li, M. Wu, Corrigendum: coagulation factor X regulated by CASC2c recruited macrophages and induced M2 polarization in glioblastoma multiforme, *Front. Immunol.* 11 (2020) 934, <https://doi.org/10.3389/fimmu.2020.00934>.
- [41] P. Micallef, M. Vujčić, Y. Wu, E. Peris, Y. Wang, B. Chanclón, A. Ståhlberg, S. L. Cardell, I. Wernstedt Asterholm, C1QTNF3 is upregulated during subcutaneous adipose tissue remodeling and stimulates macrophage chemotaxis and M1-like polarization, *Front. Immunol.* 13 (2022) 914956, <https://doi.org/10.3389/fimmu.2022.914956>.